

Taming the Energy Rise of the Total Proton-Proton Cross-Section

 Sergey Ostapchenko ^{1,2,*} and Marcus Bleicher ^{1,3}
¹ Frankfurt Institute for Advanced Studies (FIAS), 60438 Frankfurt am Main, Germany; bleicher@th.physik.uni-frankfurt.de

² D.V. Skobeltsyn Institute of Nuclear Physics, Moscow State University, 119992 Moscow, Russia

³ Institute for Theoretical Physics, Goethe-Universität, 60438 Frankfurt am Main, Germany

* Correspondence: ostapchenko@fias.uni-frankfurt.de

Received: 1 April 2019; Accepted: 4 May 2019; Published: 7 May 2019



Abstract: Steep rise of parton densities in the limit of small parton momentum fraction x poses a challenge for describing the observed energy-dependence of the total and inelastic proton-proton cross sections $\sigma_{pp}^{\text{tot/inel}}$: considering a realistic parton spatial distribution, one obtains a too-strong increase of $\sigma_{pp}^{\text{tot/inel}}$ in the limit of very high energies. We discuss various mechanisms which allow one to tame such a rise, paying special attention to the role of parton-parton correlations. In addition, we investigate a potential impact on model predictions for σ_{pp}^{tot} , related to dynamical higher twist corrections to parton-production processes.

Keywords: total cross-section; multiparton interactions; higher twist effects

1. Introduction

Modeling of high-energy collisions of hadrons is of considerable importance for experimental studies in the high-energy collider and cosmic ray fields (see, e.g., Ref. [1] for a review of the latter subject). An important part of the corresponding Monte Carlo (MC) generators is a treatment of the production of hadronic jets of relatively high transverse momenta p_t . However, because of a steep rise of parton densities in hadrons in the limit of small parton momentum fraction x , the corresponding model approaches face severe consistency problems related to a very rapid increase of both the interaction cross sections and of the yields of produced particles in the very high energy limit.

Let us start with the inclusive cross-section to produce jets of p_t larger than some chosen cutoff value $p_{t,\text{cut}}$ in pp collisions. Using the collinear factorization of the perturbative quantum chromodynamics (pQCD) [2,3], it can be expressed as a convolution of parton momentum distribution functions (PDFs) of the proton, $f_{I/p}(x, Q^2)$, with the Born parton scatter cross-section, $d\sigma_{IJ}^{2\rightarrow 2}/dp_t^2$:

$$\sigma_{pp}^{\text{jet}}(s, p_{t,\text{cut}}) = \sum_{I,J=q,\bar{q},g} \int_{p_t > p_{t,\text{cut}}} dp_t^2 \int dx^+ dx^- f_{I/p}(x^+, M_F^2) f_{J/p}(x^-, M_F^2) \frac{d\sigma_{IJ}^{2\rightarrow 2}(x^+ x^- s, p_t^2, M_F^2)}{dp_t^2}. \quad (1)$$

Here s is the center-of-mass (c.m.) energy squared for the scattering, x^\pm —light cone (LC) momentum fractions of the partons I and J [(anti-)quarks or gluons], taking part in the hard process, and M_F^2 —a chosen factorization scale. The energy rise of σ_{pp}^{jet} is thus related to the low x behavior of the PDFs $f_{I/p}(x, Q^2)$, which is driven, in turn, by the increase of the phase space for parton evolution. Describing the latter by the Dokshitzer-Gribov-Lipatov-Altarelli-Parisi (DGLAP) equations [4–6], we have approximately:

$$\sigma_{pp}^{\text{jet}}(s, p_{t,\text{cut}}) \propto \frac{1}{p_{t,\text{cut}}^2} s^{\Delta_{\text{eff}}}, \quad \Delta_{\text{eff}} \sim 0.3. \quad (2)$$

Here we immediately recognize two problems. First, the inclusive jet production cross-section depends strongly on the chosen p_t -cutoff $p_{t,cut}$. Secondly and more importantly, σ_{pp}^{jet} increases asymptotically much quicker than the total cross-section $\sigma_{pp}^{tot}(s)$, since the energy rise of the latter is bound by the unitarity and cannot be quicker than $\propto \ln^2 s$. Thus, at sufficiently high energies one inevitably deals with multiple jet production per inelastic collision, which is usually referred to as multiparton interactions (MPIs) (see, e.g., Ref. [7]).

2. Multiparton Interactions: “Minijet” Approach and Beyond

2.1. MPIs: “Minijet” Approach

Generally, the usual PDFs are insufficient to treat multiparton interactions. Rather, the corresponding formalism involves the so-called generalized multiparton distributions (“GPDs”) $F_{I_1 \dots I_n/p}^{(n)}(x_1, \dots, x_n, \vec{b}_1, \dots, \vec{b}_{n-1}, Q_1^2, \dots, Q_n^2)$ which describe a simultaneous distribution of n partons with respect to their LC momentum fractions x_i and relative transverse separations \vec{b}_i , when probed at the corresponding virtuality scales Q_i^2 [8–11]. For example, the expression for double parton scattering (DPS) cross section contains 2 GPDs $F_{I_1, I_2/p}^{(2)}$ for the projectile and target protons:

$$\begin{aligned} \sigma_{pp}^{4jet(DPS)}(s, p_{t,cut}) &= \frac{1}{2} \int dx_1^+ dx_2^+ dx_1^- dx_2^- \int_{p_{t_1}, p_{t_2} > p_{t,cut}} dp_{t_1}^2 dp_{t_2}^2 \sum_{I_1, J_2, I_1, J_2} \frac{d\sigma_{I_1 J_1}^{2 \rightarrow 2}}{dp_{t_1}^2} \frac{d\sigma_{I_2 J_2}^{2 \rightarrow 2}}{dp_{t_2}^2} \\ &\times \int d^2 \Delta b F_{I_1 I_2/p}^{(2)}(x_1^+, x_2^+, M_{F_1}^2, M_{F_2}^2, \vec{\Delta} b) F_{I_1 I_2/p}^{(2)}(x_1^-, x_2^-, M_{F_1}^2, M_{F_2}^2, \vec{\Delta} b). \end{aligned} \quad (3)$$

Here the transverse separation $\vec{\Delta} b$ between the two partons taking part in the two scattering processes is the same for the projectile and the target.

Since there exists a rather scarce experimental information on n GPDs, a standard simplifying assumption is to neglect multiparton correlations, in which case n -parton GPDs are expressed via a product of n independent single-parton GPDs:

$$F_{I_1 \dots I_n/p}^{(n)}(x_1, \dots, x_n, \vec{b}_1, \dots, \vec{b}_{n-1}, Q_1^2, \dots, Q_n^2) = \int d^2 b_n G_{I_n/p}(x_n, \vec{b}_n, Q_n^2) \prod_{i=1}^{n-1} G_{I_i/p}(x_i, \vec{b}_i + \vec{b}_n, Q_i^2), \quad (4)$$

the latter being subject to a constraint

$$\int d^2 b G_{I/p}(x, \vec{b}, Q^2) = f_{I/p}(x, Q^2). \quad (5)$$

In such a case, Equation (3) simplifies to

$$\sigma_{pp}^{4jet(DPS)}(s, p_{t,cut}) = \frac{1}{2} \int d^2 b \left[2\chi_{pp}^{jet}(s, b, p_{t,cut}) \right]^2, \quad (6)$$

being expressed via the so-called jet production eikonal χ_{pp}^{jet} , with [c.f. Equation (1)]

$$\begin{aligned} \chi_{pp}^{jet}(s, b, p_{t,cut}) &= \frac{1}{2} \sum_{I, J} \int_{p_t > p_{t,cut}} dp_t^2 \int dx^+ dx^- \int d^2 b_t G_{I/p}(x^+, \vec{b} + \vec{b}_t, M_F^2) G_{J/p}(x^-, \vec{b}_t, M_F^2) \\ &\times \frac{d\sigma_{IJ}^{2 \rightarrow 2}(x^+ x^- s, p_t^2, M_F^2)}{dp_t^2}. \end{aligned} \quad (7)$$

Here \vec{b} is the impact parameter for pp collision while \vec{b}_t refers to the transverse position of the target parton J .

More generally, for n -parton scattering one has

$$\sigma_{pp}^{\text{jet}(n)}(s, p_{t,\text{cut}}) = \frac{1}{n!} \int d^2b \left[2\chi_{pp}^{\text{jet}}(s, b, p_{t,\text{cut}}) \right]^n. \tag{8}$$

To see the effect of multiparton interactions on the total and inelastic pp cross sections, we must take into account that multiple parton scattering generates several other contributions, in addition to multiple jet production, as exemplified in Figure 1 for the particular case of DPS. The first (cut) diagram in Figure 1 corresponds to the partial contribution to σ_{pp}^{tot} from the above-discussed double-dijet production process; there are two real parton cascades giving rise to secondary hadron production. The second graph in Figure 1 describes a (negative) screening correction to single-dijet production process; in addition to the real parton cascade giving rise to hadron production, there is a virtual cascade responsible for an elastic rescattering process. Finally, the last diagram in Figure 1 corresponds to a (quasi)elastic scattering: both parton cascades are virtual ones, hence, they do not contribute to hadron production. Using the Abramovskii-Gribov-Kancheli (AGK) cutting rules [12], one obtains the relation between the relative contributions of the three graphs in Figure 1 as (+2):(-4):(+1). Consequently, the summary contribution of DPS to σ_{pp}^{tot} can be expressed via the double-dijet production cross-section as

$$\Delta^{(2)}\sigma_{pp}^{\text{tot}} = -\frac{1}{2}\sigma_{pp}^{4\text{jet(DPS)}}. \tag{9}$$

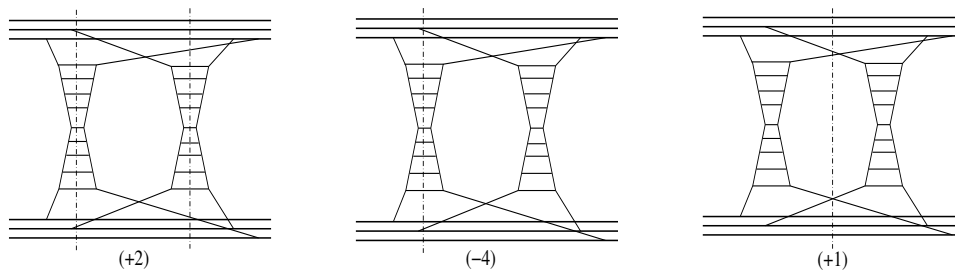


Figure 1. Schematic diagrams for different processes generated by double parton scattering in proton-proton collisions: double-dijet production (**left**), screening correction to single-dijet production (**middle**), and (quasi)elastic scattering (**right**); the vertical dashed-dotted lines indicate the position of the cut plane. Relative weights of the corresponding contributions are shown below the graphs.

It is noteworthy that the respective correction to the part of the inelastic pp cross-section, related to the production of jets of $p_t > p_{t,\text{cut}}$, $\sigma_{pp}^{\text{inel(jet)}}$, comes only from the first two graphs in Figure 1, yielding

$$\Delta^{(2)}\sigma_{pp}^{\text{inel(jet)}} = -\sigma_{pp}^{4\text{jet(DPS)}}. \tag{10}$$

Performing a similar analysis for n -parton scattering, $n > 2$, one arrives to the well-known “minijet” ansatz for $\sigma_{pp}^{\text{inel(jet)}}$ (see, e.g., Ref. [13]):

$$\sigma_{pp}^{\text{inel(jet)}}(s, p_{t,\text{cut}}) = \int d^2b \left[1 - e^{-2\chi_{pp}^{\text{jet}}(s, b, p_{t,\text{cut}})} \right], \tag{11}$$

which defines, thus, the lower bound on $\sigma_{pp}^{\text{inel}}$ and σ_{pp}^{tot} . For example, using a similar multiple scattering treatment for “soft” ($p_t < p_{t,\text{cut}}$) rescattering processes, one obtains (e.g., Ref. [14])

$$\sigma_{pp}^{\text{inel}}(s) = \int d^2b \left[1 - e^{-2\chi_{pp}^{\text{jet}}(s, b, p_{t,\text{cut}}) - 2\chi_{pp}^{\text{soft}}(s, b)} \right] \tag{12}$$

$$\sigma_{pp}^{\text{tot}}(s) = 2 \int d^2b \left[1 - e^{-\chi_{pp}^{\text{jet}}(s, b, p_{t,\text{cut}}) - \chi_{pp}^{\text{soft}}(s, b)} \right], \tag{13}$$

where the eikonal χ_{pp}^{soft} describes the contribution of such soft processes. Equations (11)–(13) form the basis for the MPI treatment in most current MC generators (see, e.g., Ref. [15] for a review).

It is important to notice that such a treatment does not modify the inclusive jet production cross-section σ_{pp}^{jet} . Indeed, summing up the partial contributions of the three graphs in Figure 1 yields

$$\Delta^{(2)}\sigma_{pp}^{\text{jet}} = \sigma_{pp}^{4\text{jet(DPS)}} [(2) * 2 + (-4) * 1 + (1) * 0] = 0, \tag{14}$$

where we take into account that the 1st graph contributes twice (two dijets produced) while the last diagram gives a zero contribution. This is known as the AGK-cancellations [12], which hold also for an arbitrary n -parton scattering. As a result, σ_{pp}^{jet} remains defined by the collinear pQCD factorization ansatz, Equation (1).

At first sight, the above-discussed eikonalization procedure allows one to “marry” the quick energy rise of σ_{pp}^{jet} with a relatively slow increase of $\sigma_{pp}^{\text{inel(jet)}}$. Since the latter depends strongly on the effective area occupied by partons in the transverse plane [c.f. Equations (7) and (11)], one seems to have a possibility to properly tune model predictions for $\sigma_{pp}^{\text{tot/inel}}$ by adjusting the energy-dependence of the spatial parton distributions. Indeed, choosing a more dilute parton distribution over a larger area at a given collision energy, as depicted in Figure 2(left), one obtains a larger $\sigma_{pp}^{\text{inel(jet)}}$ and a smaller number of jets produced per inelastic event. On the contrary, having a denser parton cloud occupying a smaller area, as in Figure 2(right), gives rise to a smaller $\sigma_{pp}^{\text{inel(jet)}}$ but to a higher jet production rate. In reality, the respective freedom is limited by experimental studies of GPDs in deep inelastic scattering (DIS) experiments and by collider measurements of the elastic scattering slope $B_{pp}^{\text{el}}(s)$ which is proportional to the average impact parameter squared for pp collision, $B_{pp}^{\text{el}} \propto \langle b^2 \rangle$, being thereby related to the effective proton size. As demonstrated in Ref. [13], using realistic parton spatial distributions in the proton results in a too fast energy rise of $\sigma_{pp}^{\text{tot/inel}}$, compared to experimental data. Current MC generators typically employ an ad hoc “solution”, assuming the jet production cutoff to be energy-dependent, $p_{t,\text{cut}} = p_{t,\text{cut}}(s)$, and empirically parametrizing such a dependence.



Figure 2. Schematic view of proton-proton collisions for a broader (left) or narrower (right) proton transverse profile.

2.2. MPIs: Role of Color Fluctuations

Potentially, the situation may be improved by considering color fluctuations in the proton [16]. Let us consider the proton to be represented by a superposition of several Fock states characterized by different spatial sizes and different parton densities, as depicted in Figure 3, i.e., $|p\rangle = \sum_i \sqrt{C_i} |i\rangle$, with C_i being the respective partial weights, $\sum_i C_i = 1$. Then Equation (11) changes to

$$\sigma_{pp}^{\text{inel(jet)}}(s, p_{t,\text{cut}}) = \sum_{i,j} C_i C_j \int d^2b \left[1 - e^{-2\chi_{pp(ij)}^{\text{jet}}(s,b,p_{t,\text{cut}})} \right], \tag{15}$$

where the eikonal $\chi_{pp(ij)}^{\text{jet}}$ describes jet production for the case when the projectile and target protons are represented by the states $|i\rangle$ and $|j\rangle$, respectively. $\chi_{pp(ij)}^{\text{jet}}$ is defined by Equation (7), with the GPDs $G_{I/p}(x, \vec{b}, Q^2)$ being replaced by the partial ones $G_{I/p(i)}(x, \vec{b}, Q^2)$, for the state $|i\rangle$ of interest, with

$$\sum_i C_i G_{I/p(i)}(x, \vec{b}, Q^2) = G_{I/p}(x, \vec{b}, Q^2). \tag{16}$$

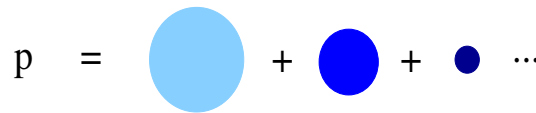


Figure 3. Schematic view for the decomposition of the proton wave function in terms of parton Fock states of different transverse sizes.

Thus, allowing for a larger dispersion between the properties of Fock states $|i\rangle$, one may reduce $\sigma_{pp}^{\text{inel(jet)}}$, hence, also $\sigma_{pp}^{\text{tot/inel}}$, for a given σ_{pp}^{jet} . Indeed, the main contribution to the total and inelastic pp cross sections comes from the largest size states of the projectile and target protons [c.f. Figures 2 and 3]. On the other hand, the above-discussed decomposition of the proton wave function has no impact on $\sigma_{pp}^{\text{jet}}(s, p_{t,\text{cut}})$: due to the constraints (5) and (16), it remains defined by Equation (1).

Yet the corresponding freedom is still rather limited by the experimental constraints discussed in Section 2.1. Additionally, a larger dispersion between the properties of proton’s Fock states gives rise to a higher cross-section for (single plus double) low mass diffraction (see, e.g., Ref. [17] for a recent discussion), which is constrained by collider measurements, notably by the TOTEM data at the Large Hadron Collider (LHC) [18,19].

It is noteworthy that taking such color fluctuations into account, one already goes beyond the simple uncorrelated parton picture. Indeed, when obtaining Equation (15), one assumes a factorization, like in Equation (4), for partial multiparton n GPDs $F_{I_1, \dots, I_n/p}^{(n)}$ for any Fock state $|i\rangle$, but Equation (4) is no longer valid for the total n GPDs $F_{I_1, \dots, I_n/p}^{(n)}$.

2.3. MPIs: Role of Multiparton Correlations

As is clear from the discussion in the previous sections, for a given inclusive jet cross-section σ_{pp}^{jet} , $\sigma_{pp}^{\text{inel(jet)}}$ anticorrelates with the average jet production rate per inelastic event. Do we have any means to further enhance the latter without changing the transverse extension of the proton profile? This turns to be possible indeed, if we reconsider the basic assumption of the minijet approach, Equation (4), and take into account multiparton correlations [20], also for particular Fock states of the proton. The main problem with the uncorrelated parton picture is illustrated qualitatively in Figure 4.



Figure 4. Schematic view for the transverse overlap of parton clouds of the colliding protons for a uniform parton distribution in the proton disk (left) and for a clumpy profile of the proton (right).

Considering, for the sake of simplicity, a top-hat transverse profile for the proton, partons are uniformly distributed in the proton disk. In such a case, multiple jet production mostly takes place in relatively central pp collisions characterized by small impact parameters, where one has a significant overlap of the projectile and target parton clouds. In turn, this results in a small average number of jets produced per inelastic event. As an alternative, one may consider a “clumpy” parton distribution, as depicted in Figure 4(right), with the parton “clumps” being created by short-range parton-parton correlations in the transverse plane. In such a picture, multiple jet production is considerably enhanced in peripheral collisions, which thus enlarges also the average jet production rate per event.

A mechanism of that kind emerges in the QGSJET-II model [21,22] which offers a combined treatment of soft and hard processes in hadronic collisions, in the framework of the so-called “semihard Pomeron” approach [23–25]. While one applies the DGLAP formalism to describe parton evolution in the region of relatively high virtualities, $|q^2| > Q_0^2$, Q_0 being some cutoff for pQCD being applicable,

nonperturbative (parts of) parton cascades, with $|q^2| < Q_0^2$, are treated phenomenologically as soft Pomeron emissions, as illustrated in Figure 5.

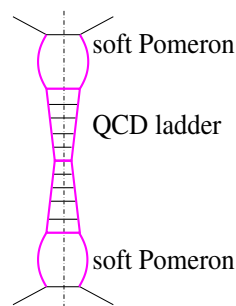


Figure 5. Schematic view of a semihard scattering process: perturbative parton evolution is represented by the ladder; the “blobs” above and below the ladder correspond to nonperturbative parton cascades described as soft Pomeron emissions.

In addition, one takes into consideration nonlinear effects related to interactions between parton cascades, which is treated as Pomeron-Pomeron interactions, the corresponding, so-called enhanced, diagrams being resummed to all orders [26–28]. As discussed in Refs. [21,29], only a subset of such enhanced diagrams can be included in the standard “minijet” framework described in Section 2.1, namely those which correspond to rescatterings of intermediate partons in the parton cascades off their parent hadrons and, thus, produce absorptive corrections to PDFs (GPDs). The other graphs, while having altogether no impact on the usual PDFs, play a crucial role in taming the energy rise of the interaction cross sections [21].

The simplest diagrams of the kind, shown in Figure 6, emerge due to a special contribution to 2 GPD of the target proton, corresponding to the so-called “soft parton splitting” mechanism [30]. Let us discuss in some detail the 1st graph in Figure 6, which defines a correction to double-dijet production. The two partons entering the two ladders from below, i.e., the initial partons for the two perturbative ($|q^2| > Q_0^2$) parton cascades, originate from two soft Pomerons describing nonperturbative parton cascading. In turn, those soft Pomerons emerge from a splitting of their parent soft Pomeron coupled to the target proton. Thus, we have the following picture: a soft parton cascade developing in the target proton, followed by a splitting of the last parton in this cascade into a pair of new soft partons which, in turn, initiate two separate soft cascades. Finally, each of those enters the perturbative ($|q^2| > Q_0^2$) domain and gives rise to a dijet production. Because of the relatively small slope of the soft Pomeron, the two partons entering the perturbative evolution appear to be close by in the transverse plane, i.e., we have effectively a parton clump. The overall (negative) corrections to $\sigma_{pp}^{\text{inel(jet)}}$ and to $\sigma_{pp}^{\text{tot/inel}}$ emerge when we add contributions of the other relevant graphs in Figure 6, similarly to the case of the eikonal double scattering [c.f. Figure 1 and Equations (9) and (10)].

It is worth remarking that in the discussed formalism, due to the AGK-cancellations, the inclusive jet production cross-section, σ_{pp}^{jet} , remains defined by the collinear pQCD factorization ansatz, Equation (1), with the PDFs $f_{I/p}(x, Q^2)$ containing absorptive corrections due to relevant enhanced diagrams [21].

Using such an approach, one is able indeed to obtain a reasonable description of both the total pp cross-section and of particle production, while using realistic PDFs and a realistic description of the spatial structure of the proton, for a fixed energy-independent cutoff¹ $Q_0^2 = 3 \text{ GeV}^2$ [22].

Concerning parton-parton correlations, one may generally expect an additional contribution coming from the so-called perturbative parton splitting mechanism which played a crucial role for properly describing the rates of high p_t double-dijet production [9,10]. This has been studied in

¹ For the chosen factorization scale, $M_{\text{F}}^2 = p_t^2/4$, this corresponds to the transverse momentum cutoff $p_{t,\text{cut}} \simeq 3.4 \text{ GeV}$.

some detail in Refs. [30,31] which showed that the corresponding contribution to $\sigma_{pp}^{4\text{jet(DPS)}}(s, p_{t,\text{cut}})$ [Equation (3)], hence, also to $\sigma_{pp}^{\text{inel(jet)}}$, is suppressed by kinematics in the limit of small $p_{t,\text{cut}}$ and can be neglected in this limit, compared to the one of the “soft parton splitting” mechanism.

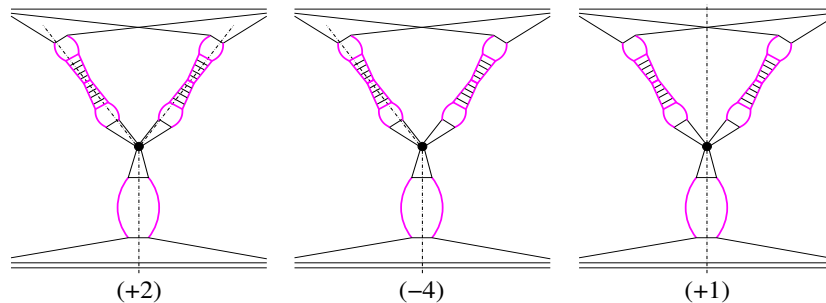


Figure 6. Schematic diagrams for the contributions of the “soft parton splitting” mechanism to double-dijet production (**left**), screening correction to single-dijet production (**middle**), and high mass diffraction of the target proton (**right**); relative weights of the contributions are shown below the graphs. Perturbative parton cascades are represented by the ladders and soft parton evolution—by the “blobs”; the triple-Pomeron interaction vertex is shown by the small black circle. The vertical dashed-dotted lines indicate the position of the cut plane.

3. Potential Importance of Dynamical Higher Twist Corrections

As stressed repeatedly in the previous Sections, a very important feature of the above-discussed approaches is that they all preserve the collinear factorization ansatz, Equation (1), for inclusive jet production. Yet this may be a problem, when applied to particle production, since the inclusive jet rates, hence, also the multiplicity of produced hadrons, depend strongly on the chosen p_t -cutoff, see Equation (2). In the QGSJET-II-04 model [22], a relatively high parton virtuality cutoff $Q_0^2 = 3 \text{ GeV}^2$ is employed as the border between the perturbative hard and nonperturbative soft parton evolution. On the other hand, from general considerations, one may expect pQCD to be applicable down to much smaller values $Q_0 \sim 1 \text{ GeV}$. Hence, an important perturbative mechanism seems to be missing.

Let us now remind ourselves that the collinear factorization of pQCD has been established at the leading power level, i.e., neglecting the so-called higher twist (HT) corrections suppressed by additional powers of the hard scale [2,3]. It is thus natural to expect that these are HT effects which damp jet production for relatively small jet transverse momenta, while being of minor importance in the high p_t range. In the following, we shall investigate the potential impact of HT corrections on the predicted interaction cross sections; applications to particle production will be discussed elsewhere [32].

While the theoretical treatment of higher twist effects dates nearly 40 years back [33–37], a rigorous implementation of the formalism in MC generators seems hardly possible at the present stage. The corresponding contributions involve many unknown multiparton correlators and generally do not allow a probabilistic treatment. Consequently, one is forced to choose a phenomenological approach and to make several brute force and, generally, ad hoc assumptions.

In the following, we are going to restrict ourselves with dynamical power corrections to hard parton scattering processes, corresponding to coherent multiple rescattering of s -channel partons on virtual soft gluons, i.e., ones characterized by vanishingly small LC momentum fractions, $x_g \sim 0$, with gluon pairs forming pair-wise color singlet states [38,39]. Such contributions have been shown to provide dominant nuclear size-enhanced corrections to the low x and low Q^2 behavior of structure functions in DIS on nuclear targets [38,40] and to the suppression of jet p_t -spectra in high-energy proton scattering on heavy nuclei, for moderately small p_t [39]. It is worth stressing that extrapolating such a treatment to proton-proton collisions is a strong ad hoc assumption since, unlike the case of a nuclear target, there is no formal justification for neglecting other potential HT contributions. We shall provide later some qualitative arguments why such an extrapolation may not be senseless.

3.1. Resummed Power Corrections to High-Energy Scattering

While traditional applications of pQCD are based on the leading twist collinear factorization [2,3], it has been demonstrated in Refs. [41,42] that such a factorization holds also for the leading, $O(1/Q^2)$, power corrections to hard scattering processes. In an example diagram of Figure 7, corresponding to the contribution to hard quark-quark scattering, which involves rescattering on two additional gluon fields, the central “blob” marked “H” depends on short distance physics only and, thus, allows a perturbative treatment. On the other hand, all the nonperturbative long distance physics is contained in multiparton correlation functions for the projectile and target hadrons, denoted by half-ellipses in the Figure, the corresponding contributions being hard process-independent. However, an implementation of such higher twist corrections in hadronic interaction models is hampered by the fact that they generally involve a considerable number of unknown multiparton correlators. Moreover, such a factorization is not expected to be valid beyond the leading power level [43,44].

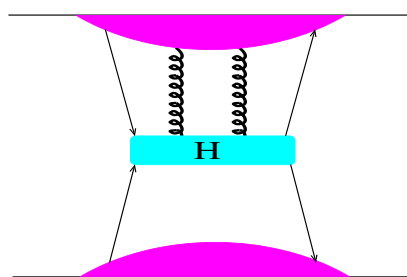


Figure 7. An example diagram for higher twist corrections discussed in the text, for the case of quark-quark hard scattering.

On the other hand, Ref. [39] demonstrated that in the high-energy (low- x) limit, dominant nuclear size-enhanced power corrections to hard scattering processes in proton-nucleus collisions come from coherent multiple rescattering of s -channel partons on virtual soft gluon pairs and that the respective contributions can be resummed to all powers. The corresponding hard scattering contributions corresponding to the “blob” H in Figure 7 have a structure exemplified in Figure 8(left) for the case of the leading power correction: two gluon fields in a pair are separated by the so-called contact part of the quark propagator, which implies no propagation in the LC-plus direction [37]; propagators which separate such gluon pairs from the quark field and from each other are represented, on the other hand, by the pole part of the propagator, which implies a propagation over considerable distances. It is such a prescription which gives rise to the nuclear enhancement: in the low x limit, the struck quark from one nucleon in the nucleus propagates over large distances $\propto 1/(x p^+)$, p^+ being the LC-plus momentum of the nucleon, scattering coherently on many correlated soft gluon pairs from other nucleons [38–40].

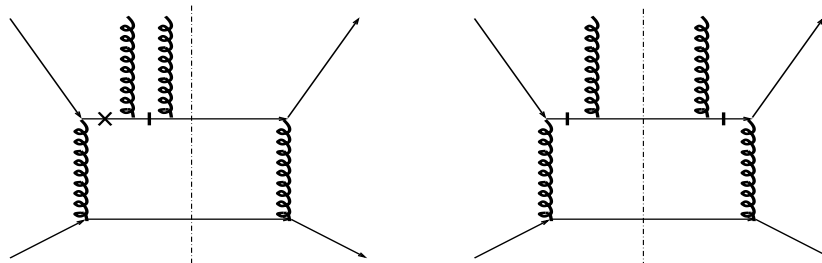


Figure 8. (Left) the structure of the hard “blob” in Figure 7, for leading power corrections discussed in the text, for the case of hard scattering of quarks of different flavors. (Right) an alternative leading power correction to the qq' hard scattering, which provides a subleading contribution in the high energy limit. Quark propagators with a vertical dash correspond to the contact terms; the propagator marked by a cross is the pole term.

In the following, we extrapolate the treatment of Ref. [39] to proton-proton collisions. The corresponding leading power (twist-4) corrections involve a quark-gluon correlation function (in the LC $A^+ = 0$ gauge)

$$T_{qg}(x, x_{g_1} = 0, x_{g_2} = 0) = \int \frac{dy_q^-}{4\pi} \frac{dy_{g_1}^- dy_{g_2}^-}{2\pi} e^{ip^+ x y_q^-} \Theta(y_{g_2}^-) \Theta(y_{g_1}^- - y_q^-) \times \langle p | \bar{\psi}(0) \gamma^+ F^{+\alpha}(y_{g_2}^-) F_\alpha^+(y_{g_1}^-) \psi(y_q^-) | p \rangle, \tag{17}$$

in the case of quark-quark or quark-gluon scattering and a similar gluon-gluon correlator T_{gg} ,

$$T_{gg}(x, x_{g_1} = 0, x_{g_2} = 0) = \int \frac{dy_g^-}{2\pi x p^+} \frac{dy_{g_1}^- dy_{g_2}^-}{2\pi} e^{ip^+ x y_g^-} \Theta(y_{g_2}^-) \Theta(y_{g_1}^- - y_g^-) \times \langle p | F^{+\beta}(0) F^{+\alpha}(y_{g_2}^-) F_\alpha^+(y_{g_1}^-) F_\beta^+(y_g^-) | p \rangle, \tag{18}$$

for gluon-quark or gluon-gluon scattering [38], with $y_q^-, y_g^-, y_{g_1}^-, y_{g_2}^-$ being the LC-minus coordinates of the fields and F_α^+ - the projection of the gluon field tensor on the LC-plus direction. Correspondingly, higher power corrections involve correlators with $2n$ gluon fields for the virtual soft gluons.

3.2. Additional Assumptions and Model Implementation

In our model implementation of the formalism discussed in Section 3.1, we make several additional strong assumptions. Starting with the quark-gluon correlator T_{qg} , a closer look at Equation (17) reveals that it formally coincides, up to a factor, with the quark-gluon ^2GPD $F_{qg}^{(2)}$ multiplied by the gluon LC momentum fraction x_g , in the limit $x_g \rightarrow 0$ and for zero transverse separation between the two partons, $\Delta b = 0$ [and, similarly, for T_{gg} in Equation (18)]. This motivated us to employ a probabilistic treatment for T_{qg} and T_{gg} , interpreting them as $x_g F_{qg}^{(2)}|_{\Delta b=0}$ and $x_g F_{gg}^{(2)}|_{\Delta b=0}$, respectively, and to proceed in a similar way with the other correlators involving larger numbers of soft gluons.

Here we must make additional assumptions concerning the relevant virtuality scales and gluon momentum fractions in the corresponding multiparton GPDs, e.g., for Q_q^2, Q_g^2 , and x_g in $F_{qg}^{(2)}(x, x_g, Q_q^2, Q_g^2, \vec{\Delta}b)$. While the natural choice for Q_q^2 is the factorization scale M_F^2 for the hard process, one usually considers soft gluons to be purely nonperturbative ones, with $Q_g^2 \sim \Lambda_{\text{QCD}}^2$. Instead, we set Q_g^2 equal to our separation scale Q_0^2 , in order to describe the GPDs by soft Pomeron asymptotics. Finally, we take into consideration that the soft gluons have a finite virtuality,

$$|q_g^2| \sim \langle p_{\vec{t}}^2 \rangle \sim x_g x_g^- s, \tag{19}$$

with x_g^- being the LC-minus fraction for the gluon and $\langle p_{\vec{t}}^2 \rangle$ - the characteristic transverse momentum squared for such soft gluons. In the factorization procedure discussed in Section 3.1, one neglects LC-minus momentum components for projectile partons (similarly neglecting LC-plus momenta of target partons) and considers the limit $x_g \rightarrow 0$ for the soft gluons involved in the process. Here, taking into account the small but finite virtuality of such gluons, Equation (19), and the fact that these gluons belong to the projectile proton (for the diagram in Figure 7), their LC-minus momentum fractions x_g^- should be much smaller than the LC-minus fraction of the target quark participating in the hard process:

$$x_g^- \sim \frac{\langle p_{\vec{t}}^2 \rangle}{x_g s} \ll x^-. \tag{20}$$

Since we expect a rather weak x_g -dependence for $x_g F_{qg}^{(2)}$ and $x_g F_{gg}^{(2)}$ in the small x_g limit at the low virtuality scale $Q_g^2 = Q_0^2$, we set

$$x_g = \frac{Q_0^2}{x^- s}. \tag{21}$$

Using these additional assumptions, the approach discussed in Section 3.1 leads to the following leading power (twist 4) correction to the inclusive jet cross-section of Equation (1)

$$\Delta^{(HT)}\sigma_{pp}^{\text{jet}}(s, p_{t,\text{cut}}) = K_{\text{HT}} \sum_{I,J=q,\bar{q},g} \int dx^+ dx^- \int d\hat{t} \Theta(\hat{t}\hat{u}/\hat{s} - p_{t,\text{cut}}^2) \frac{\pi^2 \alpha_s(M_{\text{F}}^2) C_I}{t} \times x_g F_{I_g}^{(2)}(x^+, x_g, M_{\text{F}}^2, Q_0^2, \Delta b = 0) f_{J/p}(x^-, M_{\text{F}}^2) \frac{d}{d\hat{s}} \left[\frac{\hat{s} d\sigma_{IJ}^{2\rightarrow 2}(\hat{s}, \hat{t}, M_{\text{F}}^2)}{d\hat{t}} \right], \quad (22)$$

where $\hat{s} = x^+x^-s$, \hat{t} , and $\hat{u} = -\hat{s} - \hat{t}$ are Mandelstam variables for the Born parton scattering, $x_g = Q_0^2/(x^-s)$, $C_g = C_A = 3$, $C_{q(\bar{q})} = C_F = 4/3$, and the ²GPD $F_{I_g}^{(2)}$ is taken for zero separation between the pair of projectile partons, $\Delta b = 0$. A similar correction emerges due to rescattering on soft gluons from the target proton.

Taking into consideration higher power corrections due to coherent rescattering on multiple soft gluon pairs from the projectile and the target protons, we obtain the partial jet production eikonal $\chi_{pp(ij)}^{\text{jet}}$ [c.f. Equations (15) and (7)] as

$$\begin{aligned} \chi_{pp(ij)}^{\text{jet}}(s, b, p_{t,\text{cut}}) &= \frac{1}{2} \sum_{I,J} \int dx^+ dx^- \int d^2b_t \int d\hat{t} \Theta(\hat{t}\hat{u}/\hat{s} - p_{t,\text{cut}}^2) G_{I/p(i)}(x^+, \vec{b} + \vec{b}_t, M_{\text{F}}^2) \\ &\times G_{J/p(j)}(x^-, \vec{b}_t, M_{\text{F}}^2) \left\{ 1 + \sum_{n=1}^{\infty} \frac{[K_{\text{HT}} \pi^2 \alpha_s(M_{\text{F}}^2)]^n}{n!} \left[\frac{d}{d\hat{s}} \frac{\hat{s}}{\hat{t}} \right]^n \right. \\ &\times \left. \left[\left(C_I x_g^+ G_{g/p(i)}(x_g^+, \vec{b} + \vec{b}_t, Q_0^2) \right)^n + \left(C_J x_g^- G_{g/p(j)}(x_g^-, \vec{b}_t, Q_0^2) \right)^n \right] \right\} \\ &\times \frac{d\sigma_{IJ}^{2\rightarrow 2}(\hat{s}, \hat{t}, M_{\text{F}}^2)}{d\hat{t}} \simeq \frac{1}{2} \sum_{I,J} \int dx^+ dx^- \int d^2b_t \int d\hat{t} \Theta(\hat{t}\hat{u}/\hat{s} - p_{t,\text{cut}}^2) \\ &\times \exp \left\{ \frac{K_{\text{HT}} \pi^2 \alpha_s(M_{\text{F}}^2)}{\hat{t}} \left[C_I x_g^+ G_{g/p(i)}(x_g^+, \vec{b} + \vec{b}_t, Q_0^2) + C_J x_g^- G_{g/p(j)}(x_g^-, \vec{b}_t, Q_0^2) \right] \right\} \\ &\times G_{I/p(i)}(x^+, \vec{b} + \vec{b}_t, M_{\text{F}}^2) G_{J/p(j)}(x^-, \vec{b}_t, M_{\text{F}}^2) \frac{d\sigma_{IJ}^{2\rightarrow 2}(\hat{s}, \hat{t}, M_{\text{F}}^2)}{d\hat{t}}, \quad (23) \end{aligned}$$

where $x_g^\pm = Q_0^2/(x^\mp s)$ and we approximated ⁿGPDs $F_{I_g g \dots g}^{(n)}$ (also $F_{J_g g \dots g}^{(n)}$) by factorized products of independent GPDs for the parton I and n soft gluons, taken at the same transverse position $\vec{b} + \vec{b}_t$ [c.f. Equation (4)]. Additionally, in the last step, we took into account that the HT corrections due to rescattering on soft gluon pairs from the projectile and the target are significant in different parts of the kinematic space and that the dominant contribution to parton-parton Born scattering in the high energy limit comes from a t -channel gluon exchange. Hence, we approximated the Born cross-section as

$$\frac{d\sigma_{IJ}^{2\rightarrow 2}(\hat{s}, \hat{t}, M_{\text{F}}^2)}{d\hat{t}} \simeq \frac{1}{2} C_I C_J \pi \alpha_s^2(M_{\text{F}}^2) / \hat{t}^2. \quad (24)$$

Since our treatment contains several brute force assumptions and uncertainties, we introduced an adjustable parameter, K_{HT} , which controls the magnitude of the HT corrections in our approach.

Before we present numerical results, let us provide some qualitative arguments in support of our extrapolation of the treatment of Refs. [38–40] to proton-proton collisions. Let us remind that the Lorentz-contraction acts differently on partons of different momenta, in a quickly moving parton cloud of the proton. While fast (large x) partons are confined to a narrow “pancake” in the longitudinal direction, the abundant small x gluons are spread over longitudinal distances $\propto 1/(x_g p^+)$. For the diagram in Figure 8(left), corresponding to the approach of Refs. [38–40], the low- x quark propagates over large distances $\propto 1/(x^+ p^+)$ comparable to the longitudinal size of the gluon cloud and, thus, may scatter coherently on many correlated soft gluon pairs. In contrast, considering, for example, an alternative configuration depicted in Figure 8(right), the first gluon is separated from the quark by

the contact propagator, which implies there is a very small distance between the quark and the gluon. Hence, only a very small portion of the gluon content of the proton can be involved in that type of interaction, with the corresponding contribution being a subdominant one.

3.3. Impact on the Energy Rise of pp Cross Sections

Implementing the phenomenological treatment of HT corrections, described in Section 3.2, in the framework of the QGSJET-II model, we were able to reach a consistent description of experimental data on total and elastic pp cross sections, using rather small values for the separation scale Q_0^2 between the soft and hard parton dynamics: $Q_0^2 = 1.5$ and 1 GeV^2 , which for our choice of the factorization scale, correspond to p_t -cutoff values $p_t^{\text{cut}} \simeq 2.4$ and 2 GeV , respectively. The corresponding results for σ_{pp}^{tot} , $\sigma_{pp}^{\text{inel}}$, and σ_{pp}^{el} , plotted in Figure 9 by solid lines, have been obtained using the same value $K_{\text{HT}} \simeq 4$ and suitably adjusting other model parameters. For comparison, we plot also by dashed lines the energy-dependence of these cross sections, obtained without such HT corrections, i.e., using the same two parameter sets but setting $K_{\text{HT}} = 0$. In addition, we show by dotted lines $\sigma_{pp}^{\text{inel(jet)}}$ calculated using Equation (15) in a “minijet”-like way (but including the effects of color fluctuations, as described in Section 2.2): neglecting both HT corrections and the contributions of the diagrams of the kind depicted in Figure 6 and including only those enhanced graphs which provide absorptive corrections to partial one-parton GPDs $G_{I/p(i)}(x, \vec{b}, Q^2)$. Since the rate of multiple scattering depends significantly on a chosen transverse profile for the proton (c.f. the discussion in Section 2.1), we plot additionally in Figure 10 the energy-dependence of the calculated forward elastic scattering slope, for the two parameter sets.

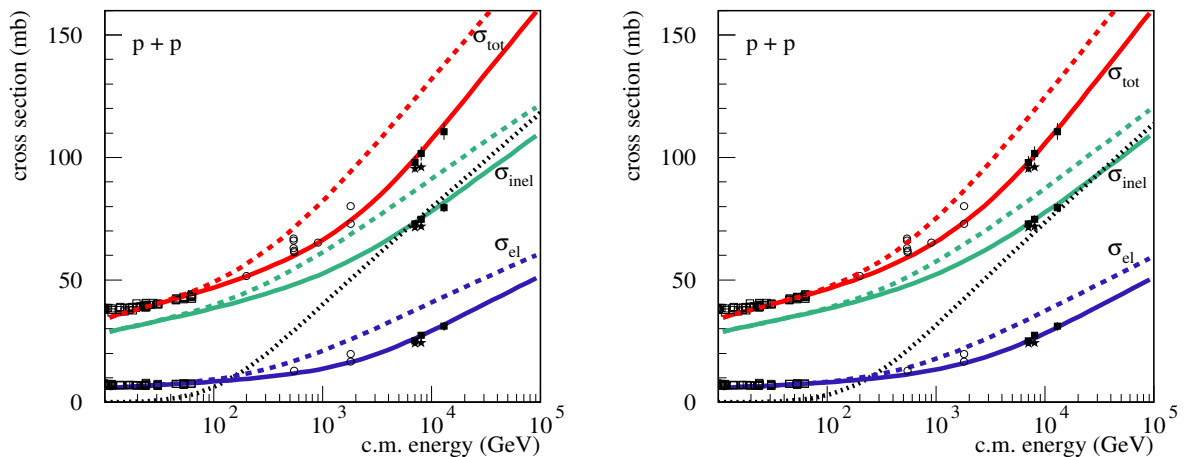


Figure 9. Energy-dependence of the calculated total, inelastic, and elastic proton-proton cross sections, for the soft-hard separation scales $Q_0^2 = 1 \text{ GeV}^2$ (left) and $Q_0^2 = 1.5 \text{ GeV}^2$ (right), obtained taking the HT corrections into account (solid lines) or neglecting them (dashed lines). The dotted lines correspond to $\sigma_{pp}^{\text{inel(jet)}}$ calculated in a “minijet”-like way, as explained in the text. The experimental data are from Refs. [45–50].

The presented results show that the above-discussed treatment of HT effects allows one indeed to reduce substantially the model dependence on the Q_0 -cutoff since the model parameters tuned to reproduce the observed energy dependences of pp cross sections differ insignificantly for the two cases considered ($Q_0^2 = 1$ and 1.5 GeV^2). Not unexpectedly, the importance of HT corrections, illustrated by the differences between the solid and dashed lines in Figure 9, increases with energy and for a smaller value of the Q_0 -cutoff. On the other hand, restricting oneself with a “minijet”-like treatment, i.e., neglecting both the “soft parton splitting” mechanism and the HT corrections to hard scattering processes, the calculated $\sigma_{pp}^{\text{inel(jet)}}$ corresponding to the part of the inelastic cross-section related to production of (mini-)jets, without the contribution of soft processes, exceeds the measured inelastic pp cross-section already at LHC energies.

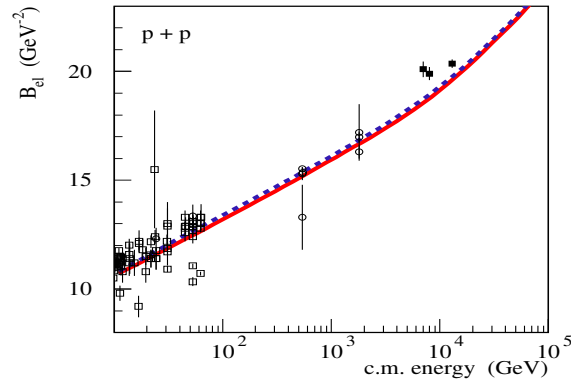


Figure 10. Energy-dependence of the calculated forward elastic scattering slope for pp collisions, for the parameter sets corresponding to the soft-hard separation scales $Q_0^2 = 1 \text{ GeV}^2$ (solid line) and $Q_0^2 = 1.5 \text{ GeV}^2$ (dashed line). The experimental data are from Refs. [45–48].

It may also be instructive to compare the x -dependence of the calculated gluon GPD, $x G_{g/p}(x, \vec{b}, Q_0^2)$, at the soft-hard separation scale Q_0^2 , for different values of b , as shown in Figures 11 and 12 by solid lines. Additionally, we plot by dotted lines the “bare” gluon GPD obtained neglecting the relevant absorptive corrections induced by Pomeron-Pomeron interactions (c.f. the discussion in Section 2.3). As discussed previously in Ref. [51] and can be seen in the figures, nonlinear effects related to Pomeron-Pomeron interactions cause a saturation of parton densities at the Q_0^2 scale, in the low x limit and for relatively small values of b . On the other hand, for increasing b , such absorptive effects become weaker and weaker, which explains the difficulty to observe signals of parton saturation in measured structure functions for DIS. It is noteworthy that the contributions of relatively large values of b to the integrated PDFs [c.f. Equation (5)], hence, also to DIS structure functions, are additionally enhanced in the low x limit by the parton transverse diffusion. It is also worth stressing here that the treatment of HT effects, discussed in Section 3.2, has no impact on PDFs (GPDs); it reduces instead the hard parton-parton scattering cross-section [c.f. Equations (22) and (23)].

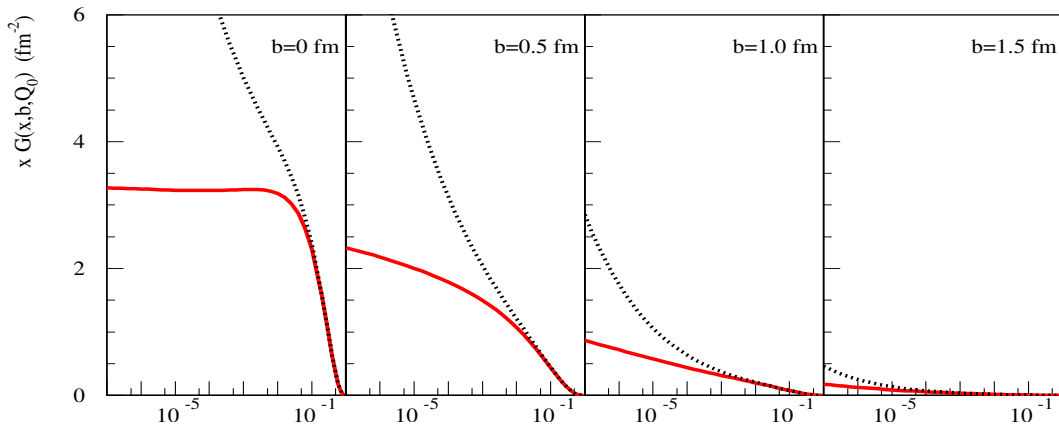


Figure 11. Calculated gluon GPD $x G_{g/p}(x, \vec{b}, Q_0^2)$ at the Q_0^2 scale for different values of b (as indicated in the plots) for the parameter set corresponding to $Q_0^2 = 1 \text{ GeV}^2$ - solid lines. $x G_{g/p}(x, \vec{b}, Q_0^2)$ calculated neglecting absorptive corrections due to Pomeron-Pomeron interactions is shown by dotted lines.

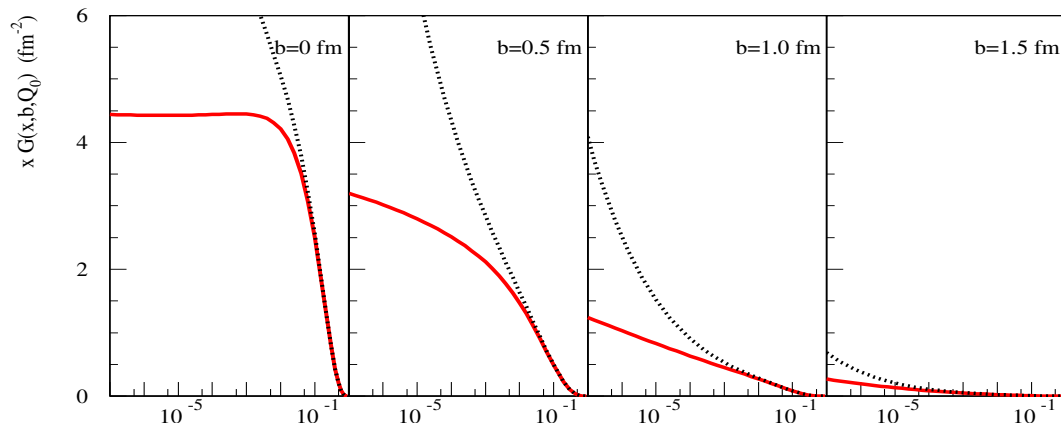


Figure 12. Same as in Figure 11 for the parameter set corresponding to $Q_0^2 = 1.5 \text{ GeV}^2$.

4. Outlook

We addressed the problem of a fast energy rise of proton-proton interaction cross sections, related to the explosive increase of the inclusive (mini-)jet production rate in the high energy limit, which, in turn, stems from the steep low- x rise of parton densities in hadrons. We demonstrated that common difficulties in “marrying” experimental data on the low- x behavior of the gluon PDF in the proton with the moderate energy-dependence of the total pp cross-section is mainly related to the basic assumption of the popular “minijet” approach: using uncorrelated parton picture, both in momentum and transverse coordinate space, for multiple scattering processes. Taking into account parton-parton correlations, in particular, those produced by the “soft parton splitting” mechanism, allows one to substantially improve the situation.

This is, however, insufficient to obtain a reasonable matching between the treatments of soft and hard processes in the corresponding models of high-energy hadronic interactions: the predictions for interaction cross sections and, especially, for particle production depend strongly on the chosen separation scale, the so-called Q_0 -cutoff, between the soft and hard physics. In that respect, the situation may be improved by taking into consideration dynamical higher twist corrections to hard parton scattering processes. In this work, we proposed a phenomenological treatment of such corrections, relating them to generalized parton distributions in the proton, with allowed us, using a single additional adjustable parameter, to substantially reduce the dependence of the model results on the Q_0 -cutoff.

It is noteworthy that our treatment is qualitatively similar to the popular recipe used in most present MC generators: the use of an energy-dependent cutoff for jet production. Indeed, in our approach, the taming of the wild energy rise of pp cross sections is due to a suppression of hard scattering processes, for relatively small transverse momenta of produced final partons, rather than due to a modification of PDFs, related to parton saturation. On the other hand, due to the assumed relation to parton GPDs, we have a dynamical treatment, e.g., the corresponding corrections become stronger for more central proton-proton collisions.

Yet the proposed approach is a highly phenomenological one and involves numerous brute force assumptions. Hence, further cross checks and constraints, notably, based on experimental data for secondary particle production, are highly desirable. In particular, an independent calibration of the basic parameter of the scheme, which controls the magnitude of the respective corrections, e.g., based on measured hadron transverse spectra in the range of moderately small p_t [52], is required.

Author Contributions: Both authors contributed equally to the work.

Funding: This research was funded in part by Deutsche Forschungsgemeinschaft (project OS 481/2-1) and by the State of Hesse via the LOEWE-Center HIC for FAIR.

Conflicts of Interest: The authors declare no conflict of interest.

Abbreviations

The following abbreviations are used in this manuscript:

MDPI	Multidisciplinary Digital Publishing Institute
MC	Monte Carlo
pQCD	perturbative quantum chromodynamics
PDF	parton distribution function
LC	light cone
c.m.	center-of-mass
DGLAP	Dokshitzer-Gribov-Lipatov-Altarelli-Parisi
MPI	multiparton interaction
GPD	generalized parton distribution
DPS	double parton scattering
AGK	Abramovskii-Gribov-Kancheli
DIS	deep inelastic scattering
LHC	Large Hadron Collider
HT	higher twist

References

- Engel, R.; Heck, D.; Pierog, T. Extensive air showers and hadronic interactions at high energy. *Ann. Rev. Nucl. Part. Sci.* **2011**, *61*, 467–489. [[CrossRef](#)]
- Collins, J.C.; Soper, D.E.; Sterman, G.F. Soft Gluons and Factorization. *Nucl. Phys. B* **1988**, *308*, 833–856. [[CrossRef](#)]
- Collins, J.C.; Soper, D.E.; Sterman, G.F. Factorization of Hard Processes in QCD. *Adv. Ser. Direct. High Energy Phys.* **1989**, *5*, 1–91.
- Gribov, V.N.; Lipatov, L.N. Deep inelastic e p scattering in perturbation theory. *Sov. J. Nucl. Phys.* **1972**, *15*, 438–450.
- Altarelli, G.; Parisi, G. Asymptotic Freedom in Parton Language. *Nucl. Phys. B* **1977**, *126*, 298–318. [[CrossRef](#)]
- Dokshitzer, Y.L. Calculation of the Structure Functions for Deep Inelastic Scattering and e^+e^- Annihilation by Perturbation Theory in Quantum Chromodynamics. *Sov. Phys. JETP* **1977**, *46*, 641–653.
- Akiba, K.; Akbiyik, M.; Albrow, M.; Arneodo, M.; Avati, V.; Baechler, J.; Baillie, O.V.; Bartalini, P.; Bartels, J.; Baur, S.; et al. LHC Forward Physics. *J. Phys. G* **2016**, *43*, 110201. [[CrossRef](#)]
- Calucci, G.; Treleani, D. Incoherence and multiple parton interactions. *Phys. Rev. D* **2009**, *80*, 054025. [[CrossRef](#)]
- Blok, B.; Dokshitzer, Y.; Frankfurt, L.; Strikman, M. The Four jet production at LHC and Tevatron in QCD. *Phys. Rev. D* **2011**, *83*, 071501. [[CrossRef](#)]
- Blok, B.; Dokshitzer, Y.; Frankfurt, L.; Strikman, M. pQCD physics of multiparton interactions. *Eur. Phys. J. C* **2012**, *72*, 1963. [[CrossRef](#)]
- Diehl, M.; Ostermeier, D.; Schafer, A. Elements of a theory for multiparton interactions in QCD. *JHEP* **2012**, *1203*, 89. [[CrossRef](#)]
- Abramovsky, V.A.; Gribov, V.N.; Kancheli, O.V. Character of Inclusive Spectra and Fluctuations Produced in Inelastic Processes by Multi-Pomeron Exchange. *Sov. J. Nucl. Phys.* **1974**, *18*, 308–316.
- Rogers, T.C.; Stasto, A.M.; Strikman, M.I. Unitarity Constraints on Semi-hard Jet Production in Impact Parameter Space. *Phys. Rev. D* **2008**, *77*, 114009. [[CrossRef](#)]
- Durand, L.; Pi, H. Semihard QCD and High-energy pp and $\bar{p}p$ Scattering. *Phys. Rev. D* **1989**, *40*, 1436. [[CrossRef](#)]
- Wang, X.-N. pQCD based approach to parton production and equilibration in high-energy nuclear collisions. *Phys. Rept.* **1997**, *280*, 287–371. [[CrossRef](#)]
- Frankfurt, L.; Strikman, M.; Treleani, D.; Weiss, C. Evidence for color fluctuations in the nucleon in high-energy scattering. *Phys. Rev. Lett.* **2008**, *101*, 202003. [[CrossRef](#)]
- Khoze, V.A.; Martin, A.D.; Ryskin, M.G. Elastic and diffractive scattering at the LHC. *Phys. Lett. B* **2018**, *784*, 192. [[CrossRef](#)]

18. Antchev, G.; Berretti, M.; Bozzo, M.; Brogi, P.; Robutti, E.; Smajek, J.; Radicioni, E.; Atanassov, I.; Ferretti, R.; Eggert, K.; et al. Measurement of proton-proton inelastic scattering cross-section at $\sqrt{s} = 7$ TeV. *Europhys. Lett.* **2013**, *101*, 21003.
19. Antchev, G.; Aspell, P.; Atanassov, I.; Avati, V.; Baechler, J.; Berardi, V.; Berretti, M.; Bossini, E.; Bottigli, U.; Bozzo, M.; et al. Double diffractive cross-section measurement in the forward region at the LHC. *Phys. Rev. Lett.* **2013**, *111*, 262001. [[CrossRef](#)]
20. Rogers, T.C.; Strikman, M. Multiple Hard Partonic Collisions with Correlations in Proton-Proton Scattering. *Phys. Rev. D* **2010**, *81*, 016013. [[CrossRef](#)]
21. Ostapchenko, S. Nonlinear screening effects in high energy hadronic interactions. *Phys. Rev. D* **2006**, *74*, 014026. [[CrossRef](#)]
22. Ostapchenko, S. Monte Carlo treatment of hadronic interactions in enhanced Pomeron scheme: QGSJET-II model. *Phys. Rev. D* **2011**, *83*, 014018. [[CrossRef](#)]
23. Drescher, H. J.; Hladik, M.; Ostapchenko, S.; Werner, K. A Unified treatment of high-energy interactions. *J. Phys. G* **1999**, *25*, L91. [[CrossRef](#)]
24. Drescher, H.J.; Hladik, M.; Ostapchenko, S.; Pierog, T.; Werner, K. Parton based Gribov-Regge theory. *Phys. Rep.* **2001**, *350*, 93–289. [[CrossRef](#)]
25. Ostapchenko, S.; Drescher, H.J.; Liu, F.M.; Pierog, T.; Werner, K. Consistent treatment of soft and hard processes in hadronic interactions. *J. Phys. G* **2002**, *28*, 2597. [[CrossRef](#)]
26. Ostapchenko, S. On the re-summation of enhanced Pomeron diagrams. *Phys. Lett. B* **2006**, *636*, 40–45. [[CrossRef](#)]
27. Ostapchenko, S. Enhanced Pomeron diagrams: Re-summation of unitarity cuts. *Phys. Rev. D* **2008**, *77*, 034009. [[CrossRef](#)]
28. Ostapchenko, S. Total and diffractive cross sections in enhanced Pomeron scheme. *Phys. Rev. D* **2010**, *81*, 114028. [[CrossRef](#)]
29. Ryskin, M.G.; Martin, A.D.; Khoze, V.A. Soft processes at the LHC. II. Soft-hard factorization breaking and gap survival. *Eur. Phys. J. C* **2009**, *60*, 265–272. [[CrossRef](#)]
30. Ostapchenko, S.; Bleicher, M. Double parton scattering: Impact of nonperturbative parton correlations. *Phys. Rev. D* **2016**, *93*, 034015. [[CrossRef](#)]
31. Blok, B.; Strikman, M. Interplay of soft and perturbative correlations in multiparton interactions at central rapidities. *Phys. Lett. B* **2017**, *772*, 219–224. [[CrossRef](#)]
32. Ostapchenko, S.; Bleicher, M. A dynamical cutoff on low p_t jet production from higher twist effects. 2019, paper in preparation.
33. Jaffe, R.L.; Soldate, M. Twist Four in the QCD Analysis of Leptoproduction. *Phys. Lett. B* **1981**, *105B*, 467–472. [[CrossRef](#)]
34. Jaffe, R.L.; Soldate, M. Twist Four in Electroproduction: Canonical Operators and Coefficient Functions. *Phys. Rev. D* **1982**, *26*, 49. [[CrossRef](#)]
35. Ellis, R.K.; Furmanski, W.; Petronzio, R. Power Corrections to the Parton Model in QCD. *Nucl. Phys. B* **1982**, *207*, 1–14. [[CrossRef](#)]
36. Ellis, R.K.; Furmanski, W.; Petronzio, R. Unraveling Higher Twists. *Nucl. Phys. B* **1983**, *212*, 29. [[CrossRef](#)]
37. Qiu, J.-W. Twist Four Contributions to the Parton Structure Functions. *Phys. Rev. D* **1990**, *42*, 30. [[CrossRef](#)]
38. Qiu, J.-W.; Vitev, I. Resummed QCD power corrections to nuclear shadowing. *Phys. Rev. Lett.* **2004**, *93*, 262301. [[CrossRef](#)]
39. Qiu, J.-W.; Vitev, I. Coherent QCD multiple scattering in proton-nucleus collisions. *Phys. Lett. B* **2006**, *632*, 507–511. [[CrossRef](#)]
40. Qiu, J.-W.; Vitev, I. Nuclear shadowing in neutrino nucleus deeply inelastic scattering. *Phys. Lett. B* **2004**, *587*, 52–61. [[CrossRef](#)]
41. Qiu, J.-W.; Serman, G. Power corrections in hadronic scattering. 1. Leading $1/Q^{*2}$ corrections to the Drell-Yan cross-section. *Nucl. Phys. B* **1991**, *353*, 105–136. [[CrossRef](#)]
42. Qiu, J.-W.; Serman, G. Power corrections to hadronic scattering. 2. Factorization. *Nucl. Phys. B* **1991**, *353*, 137–164. [[CrossRef](#)]
43. Doria, R.; Frenkel, J.; Taylor, J.C. Counter Example to Nonabelian Bloch-Nordsieck Theorem. *Nucl. Phys. B* **1980**, *168*, 93. [[CrossRef](#)]

44. Basu, R.; Ramalho, A.J.; ; Sterman, G. Factorization at Higher Twist in Hadron—Hadron Scattering. *Nucl. Phys. B* **1984**, *244*, 221–246. [[CrossRef](#)]
45. Nakamura, K.; Hagiwara, K.; Hikasa, K.; Murayama, H.; Tanabashi, M.; Watari, T.; AMSLER, C.; Antonelli, M.; Asner, D.M.; Baer, H.; et al. Review of particle physics. *J. Phys. G* **2010**, *37*, 075021. [[CrossRef](#)]
46. Antchev, G.; Aspell, P.; Atanassov, I.; Avati, V.; Baechler, J.; Berardi, V.; Berretti, M.; Bossini, E.; Bozzo, M.; Brogi, P.; et al. Luminosity-independent measurements of total, elastic and inelastic cross-sections at $\sqrt{s} = 8$ TeV. *Europhys. Lett.* **2013**, *101*, 21004.
47. Antchev, G.; Aspell, P.; Atanassov, I.; Avati, V.; Baechler, J.; Berardi, V.; Berretti, M.; Bossini, E.; Bottigli, U.; Bozzo, M.; et al. Luminosity-Independent Measurement of the Proton-Proton Total Cross Section at $\sqrt{s} = 8$ TeV. *Phys. Rev. Lett.* **2013**, *111*, 012001. [[CrossRef](#)]
48. Antchev, G.; Aspell, P.; Atanassov, I.; Avati, V.; Baechler, J.; Barrera, C.B.; Berardi, V.; Berretti, M.; Bossini, E.; Bottigli, U.; et al. First measurement of elastic, inelastic and total cross-section at $\sqrt{s} = 13$ TeV by TOTEM and overview of cross-section data at LHC energies. *Eur. Phys. J. C* **2019**, *79*, 103. [[CrossRef](#)]
49. ATLAS Collaboration. Measurement of the total cross section from elastic scattering in pp collisions at $\sqrt{s} = 7$ TeV with the ATLAS detector. *Nucl. Phys. B* **2014**, *889*, 486. [[CrossRef](#)]
50. ATLAS Collaboration. Measurement of the total cross section from elastic scattering in pp collisions at $\sqrt{s} = 8$ TeV with the ATLAS detector. *Phys. Lett. B* **2016**, *761*, 158. [[CrossRef](#)]
51. Ostapchenko, S. Non-linear effects in high energy hadronic interactions. *arXiv* **2005**, arXiv:hep-ph/0501093.
52. CMS Collaboration. Production of leading charged particles and leading charged-particle jets at small transverse momenta in pp collisions at $\sqrt{s} = 8$ TeV. *Phys. Rev. D* **2015**, *92*, 112001. [[CrossRef](#)]



© 2019 by the authors. Licensee MDPI, Basel, Switzerland. This article is an open access article distributed under the terms and conditions of the Creative Commons Attribution (CC BY) license (<http://creativecommons.org/licenses/by/4.0/>).